RSC Advances

RSC Publishing

PAPER

View Article Online
View Journal | View Issue

Cite this: *RSC Adv.*, 2013, **3**, 25891

Synthesis of carbon nano-onion and nickel hydroxide/oxide composites as supercapacitor electrodes

Marta E. Plonska-Brzezinska,*[a] Diana M. Brus,[a] Agustín Molina-Ontoria[b] and Luis Echegoyen*[b]

Received 8th August 2013
Accepted 10th October 2013

DOI: 10.1039/c3ra44249g

www.rsc.org/advances

"Small" carbon nano-onions (CNOs) are spherical, *ca.* 5 nm in diameter, concentric shells of graphitic carbon that can be also described as multi-shelled fullerenes. Given the easy functionalization and high thermal stability of the CNOs produced from nanodiamond, they are the most obvious choice for studying the potential applications of these multi-shelled fullerenes in electrochemical supercapacitors (ES). Since limited accessibility of the carbon surface to electrolyte penetration is observed for carbon nano-onions, performance enhancement was accomplished by modifying the CNO surfaces with pseudocapacitive redox materials: $Ni(OH)_2$ and NiO. These composites were characterized by TEM, SEM, XRD, TGA-DTG-DTA and Raman spectroscopy. The electrochemical properties of these composites were also investigated. Compared with pristine CNOs (30.6 F g^{-1} at 5 mV s^{-1}), modified CNOs (1225.2 F g^{-1} for CNOs/$Ni(OH)_2$ and 290.6 F g^{-1} for CNOs/NiO, both at 5 mV s^{-1}) show improved electrochemical performance, promising for the development of supercapacitors.

1. Introduction

An electrochemical capacitor, also called an electrochemical supercapacitor (ES) or ultracapacitor, is a device able to store charge at the electrode–electrolyte interface.[1] This accumulation of charge is mainly based on two types of processes: electrostatic interactions (electrical double layer capacitors, EDLC),[2] or faradaic processes (pseudocapacitors, also called faradaic supercapacitors, FS).[3] In EDLCs the energy can be stored *via* ion adsorption and the capacitance is associated with an electrode-potential-dependent accumulation of charge at the electrode interface through polarization. During the charging–discharging process of carbon-based EDLCs, the electrode material is not electrochemically active. In pseudocapacitors the electrode material is electrochemically active and faradaic reactions take place, which are also involved in the charge storage/delivery process. The type of charge storage mechanism determines the electrochemical performance of ECs and the electrode materials are also crucial. Ideal electrode materials are required to possess: a high specific surface area, controlled porosity, high charge exchange rates, high electronic conductivity, good power density, high thermal and chemical stability, and preferably low costs of the raw materials and manufacturing.[4,5]

Many systems have been developed as electrode materials for supercapacitors. Pseudocapacitors are generally classified into two types: conductive polymers[6] and electroactive transition-metal oxides/hydroxides.[7] Conductive polymers have been widely investigated for fabricating supercapacitors, because they have multiple redox states, good environmental stability, and they are inexpensively and easily fabricated into various nanostructures.[8] However, they usually suffer from degradation resulting from the repeated charge–discharge processes, leading to poor cycling performance. To improve the specific capacitance and the energy density, transition metal oxides/hydroxides are being investigated as alternative materials for supercapacitor electrodes. Generally, using metal oxides/hydroxides in ES requires: (i) electronic conductivity, (ii) two or more oxidation states that coexist over a continuous potential range with no phase changes and (iii) protons to intercalate into the oxide lattice upon reduction (and out of the lattice upon oxidation).[9] To date, the systems investigated include oxides/hydroxides of ruthenium,[10] manganese,[11] cobalt,[12] nickel,[13] and vanadium.[14] These materials exhibit reasonable pseudocapacitive performance. On the other hand, metal oxides/hydroxides may not be employed alone as supercapacitor electrodes due to: (i) very low conductivity, (ii) poor power density, (iii) low charge exchange rates, (iv) poor long-term stability during the charge–discharge processes that lead to cracking of the electrode, and (v) low surface area and non-homogeneous pore distributions.

Nickel oxide/hydroxide is one of the most widely used materials in pseudocapacitors. It has been determined that $Ni(OH)_2$ can yield much higher specific capacitances than NiO.[15] Nanostructures with different morphologies like wires,

[a]*Institute of Chemistry, University of Bialystok, Hurtowa 1, 15-399 Bialystok, Poland. E-mail: mplonska@uwb.edu.pl; Fax: +48 85 747 0113; Tel: +48 85 745 7816*

[b]*Department of Chemistry, University of Texas at El Paso, 500 W. University Ave., El Paso, TX 79968, USA. E-mail: echegoyen@utep.edu; Fax: +1 915 747 6801; Tel: +1 915 747 7573*

urchins, cones, balls with ripple-shaped pores, and belts have been fabricated and tested.[16] The specific capacitance of the nickel hydroxides depend on the structures, but all exhibit values that are far from their theoretical maximum, 2573 F g^{-1} at 0.5 V,[17] depending on the synthesis method and the morphology.[18] Therefore, it is important to investigate how to maximize the electrochemical performance of nickel hydroxide. For instance, a high specific capacitance of 1478 F g^{-1} with excellent charge exchange rates and long cycle ability was obtained for a nickel hydroxide film calcinated at 250 °C.[19] The typical specific capacitance based on nickel hydroxide electrodes ranges from 50 to 1776 F g^{-1}.[20] To our knowledge, the highest specific capacitance, 3152 F g^{-1}, was achieved for electrodeposited $Ni(OH)_2$ on nickel foam in a 3% KOH solution at a charge–discharge current density of 4 A g^{-1}.[21]

The electrochemical performance of pseudocapacitors depends mainly on the synthetic procedures used. Several synthetic strategies can be exploited to fabricate mixed-composites containing metal oxides including hydrothermal synthesis,[22] sol–gel chemistry,[23] electrodeposition[24] or spray pyrolysis.[25] The method allows to control electrode microstructures, morphology and homogeneity. Recently, work with supercapacitors has been focused on designing and synthesizing composite electrode materials to fully exploit their advantages and overcome their disadvantages. Some reports showed that high specific capacitances can be obtained if metal oxides or hydroxides are uniformly dispersed on carbon materials with high surface areas.[26] Combining metal oxide/hydroxide with carbon nanomaterials could: enhance specific surface areas, induce high porosity, facilitate electron and proton conduction, expand active sites, extend the potential window, protect active materials from mechanical degradation, improve cycling stability and provide extra pseudocapacitance. Various carbon-based composites are currently being investigated as supercapacitor electrodes because of the synergistic properties arising from the carbon materials (high power density) and from the pseudo-capacitive nanomaterials (high energy density),[27] including nickel oxides/hydroxides.[28]

New types of supercapacitors which combine the advantages of both double layer capacitors and pseudocapacitors are the subject of this work. To the best of our knowledge, this is the first composite synthesis of "small" carbon nano-onions (CNOs) with nickel oxides/hydroxides. The CNO structures consist of a hollow spherical fullerene core surrounded by concentric and curved graphene layers with increasing diameters. The high temperature annealing of ultra-dispersed nanodiamonds (5 nm, average size) leads to their transformation into CNO structures (5–6 nm in diameter, 6–8 shells).[29] The interest in carbon nano-onions is driven by their unusual physico-chemical properties as well as by promising applications in electronics,[30,31] optics,[32] biosensors,[33] as hyperlubricants,[34] and in energy conversion and storage.[35]

The number of published articles describing CNO composite preparation is still very sparse. Non-modified CNOs have limited charge accumulation properties. Combining the carbon material with an inorganic one should lead to electrochemical properties from both of them. The fast charging rate capability of nickel hydroxide and oxide is associated with rapid proton diffusion in the $Ni(OH)_2$ and NiO frameworks.[36] In order to obtain a high charge exchange rate, it is necessary to prepare nanosized inorganic materials. Recently, the design of a new type of NiO/C nanocapsule with onion-like C shells was published which exhibited a high charge–discharge rate and an excellent cycling stability.[37]

In the present work, CNO/$Ni(OH)_2$ composites were prepared by loading of $Ni(OH)_2$ on the carbon structures, followed by calcination to obtain CNO/NiO. The composites were characterized by TEM, SEM, XRD, TGA-DTG-DTA, FT-IR and Raman spectroscopy. The electrochemical properties of the hybrid systems in an aqueous electrolyte were also examined.

2. Experimental section

2.1. Materials

The following chemicals were used as received: nickel(II) nitrate hexahydrate (>97.0%, Sigma-Aldrich), ethyl alcohol absolute (99.8%, POCH), ammonia hydrate (25%, POCH), conductive carbon paint – a dispersion of colloidal graphite (20% solids) in isopropyl alcohol, polyvinylpyrrolidone (PVP) (≥99.0%, Sigma-Aldrich), (4-dimethylamino)pyridine (4-DMAP) (≥99.0%, Sigma-Aldrich), pyridinium *p*-toluenesulfonate polymer-bound (PPST) (Sigma-Aldrich), nanodiamond powder (Carbodeon uDiamond® Molto) with a crystal size between 4 and 6 nm, and nanodiamond content ≥97 wt%.

Commercially available nanodiamond powder with a crystal size between 4 and 6 nm was used for the preparation of CNOs. NDs were placed in a graphite crucible and transferred to an Astro carbonization furnace. The air in the furnace was removed by applying a vacuum followed by purging with helium. The process was repeated twice to ensure complete removal of air. Annealing of ultradispersed nanodiamonds was performed at 1650 °C under a 1.1 MPa He atmosphere with a heating ramp of 20 °C min^{-1}.[15] The final temperature was maintained for one hour, then the material was slowly cooled to room temperature over a period of one hour. The furnace was opened, and the CNOs were annealed in air at 400 °C to remove any amorphous carbon.

All aqueous solutions for electrochemical studies were prepared using deionized water of 18.2 MΩ resistivity, which was further purified with a Milli-Q system (Millipore).

2.2. Synthesis of nickel hydroxide

5 g of nickel nitrate hexahydrate was dissolved in 40 mL of water and ethanol in a volume 1 : 1 ratio and stirred. To this solution was added 5% ammonia hydrate dropwise to achieve a pH = 9.5. The precipitate was centrifuged and washed several times with ethanol to remove ammonia hydrate. The resulting aquamarine solid was dried overnight in an oven at 60 °C.

50 mg of the selected substance, PVP, 4-DMAP or PPST, was dissolved in a mixture (40 mL) of water and anhydrous ethanol in a 1 : 1 ratio and sonicated for 15 minutes. Subsequently, 5 g of nickel nitrate hexahydrate was dispersed in this solution and stirred. During stirring, 5% ammonia hydrate solution was added dropwise until the pH = 9.5. The suspension was

centrifuged. The precipitate was collected and washed several times with ethanol. Finally, the crude product was dried overnight in an oven at 60 °C.

2.3. Preparation of composites of CNOs/4-DMAP/Ni(OH)$_2$

10 mg of CNOs was dispersed in 3 mL of anhydrous ethanol and mixed with 3 mL of an aqueous solution of (4-dimethylamino) pyridine (5 mg). This suspension was placed in an ultrasonic bath for 15 minutes. Nickel nitrate hexahydrate (500 mg) was then added and the mixture was stirred. A 5% ammonium hydroxide solution was then added dropwise to the suspension until the pH was 9.5. The solution was stirred and the black solid on the bottom of the eppendorfs was separated from the blue solution by centrifugation. This composite material was washed several times with ethanol until the solvent was transparent. Subsequently, it was dried overnight in an oven at 60 °C. The composite of CNOs/4-DMAP/Ni(OH)$_2$ with a mass ratio of CNOs to Ni(OH)$_2$ about 4 : 1 was thus obtained. The composites with nickel oxide (CNOs/4-DMAP/NiO) were obtained by calcination of CNOs/4-DMAP/Ni(OH)$_2$ in an autoclave at 300 °C during 2 hours.

2.4. Apparatus

The products and composite films were imaged by secondary electron SEM with the use of a INSPECT S50 scanning electron microscope from FEI. The accelerating voltage of the electron beam was 15 keV and the working distance was 10 mm. Transmission electron microscopy analyses were performed with a FEI instrument operated at 200 kV. The materials were sonicated in ethanol for 30 min and deposited on copper grids. Powder X-ray diffraction (XRD) (X'Pert Pro, Panalytica) were obtained using a Cu K_α source at a scanning speed of 0.0067° s^{-1} over a 2 Theta range of 10–90°. Thermogravimetric experiments were performed using an SDT 2960 simultaneous TGA-DTG-DTA (TA Instruments company). The spectra were collected at 10 °C min^{-1} in an air atmosphere (100 mL min^{-1}). The Fourier Transform Infrared (FTIR) spectra were recorded between 4000 and 100 cm^{-1} with a Nicolet 6700 Thermo Scientific spectrometer at room temperature and a N_2 atmosphere. The spectra were collected with a resolution of 4 cm^{-1}. All the spectra were corrected using conventional software in order to cancel the variation of the analyzed thickness with the wavelength. The room-temperature Raman spectra at wavelengths between 100 and 3500 cm^{-1} were investigated using a Renishaw spectrometer. To avoid sample overheating, the power of the laser beam was reduced to about 3 mW. The positions of the Raman peaks were calibrated using a Si thin film as an external standard. The spectral resolution of the Raman spectra was 2 cm^{-1}.

The electrochemical measurements were obtained using a three-electrode configuration and a computer-controlled Autolab modular electrochemical system (Eco Chemie Ultecht, The Netherlands), using GPES software (Eco Chemie Ultecht). The working electrode was a glassy carbon (GC) disk electrode (Bioanalytical System Inc.) with a disk diameter of 2 mm. Prior to the measurements the glassy carbon electrode was polished with alumina powder on polishing cloth. The electrode was immersed in ethanol, sonicated for a few minutes and washed with water to remove all impurities. The film on the GC electrode was prepared as follows: 2 mg of active material was dissolved in a solution containing conductive carbon paint and ethanol in a volume ratio of 1 : 6 and sonicated for 15 minutes. Subsequently, the surface of the working electrode was modified by the drop-coating method. A saturated calomel electrode (SCE) was used as the reference electrode and a Pt wire served as the counter electrode. The electrochemical measurements were performed in 1 M KOH aqueous electrolyte at room temperature and under an argon atmosphere. Cyclic voltammograms (CV) were measured between −0.6 and 0.6 V (*vs.* SCE) and −0.6 to 0 (*vs.* SCE) at different scan rates.

3. Results and discussion

3.1. Preparation and characterization of Ni(OH)$_2$ and NiO

The synthesis of the precursors, Ni(OH)$_2$ and NiO, in the presence of the different pyridine derivatives was performed. Three different modifiers were employed for Ni(OH)$_2$ preparation, polyvinylpyrrolidone (PVP), (4-dimethylamino)pyridine (4-DMAP) and pyridinium *p*-toluenesulfonate polymer-bound (PPST) (Scheme 1). A control reaction was performed without any modifier (Scheme 1a (1)).

The results confirmed that this method offers a versatile means to fabricate Ni(OH)$_2$ nanostructures with different morphologies (Fig. 1). The formation process of Ni(OH)$_2$ occurs by the following steps:[38]

$$Ni^{2+} + NH_3H_2O \rightarrow [Ni(NH_3)_y]^{2+} + yH_2O \quad (1)$$

$$[Ni(NH_3)_y]^{2+} \rightarrow Ni^{2+} + yNH_3 \quad (2)$$

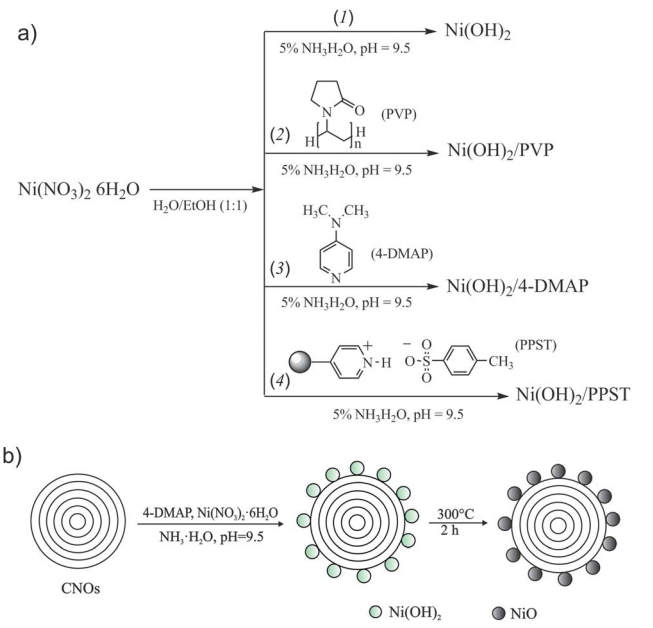

Scheme 1 Synthesis of (a) Ni(OH)$_2$, (b) CNO/4-DMAP/Ni(OH)$_2$ and CNO/4-DMAP/NiO.

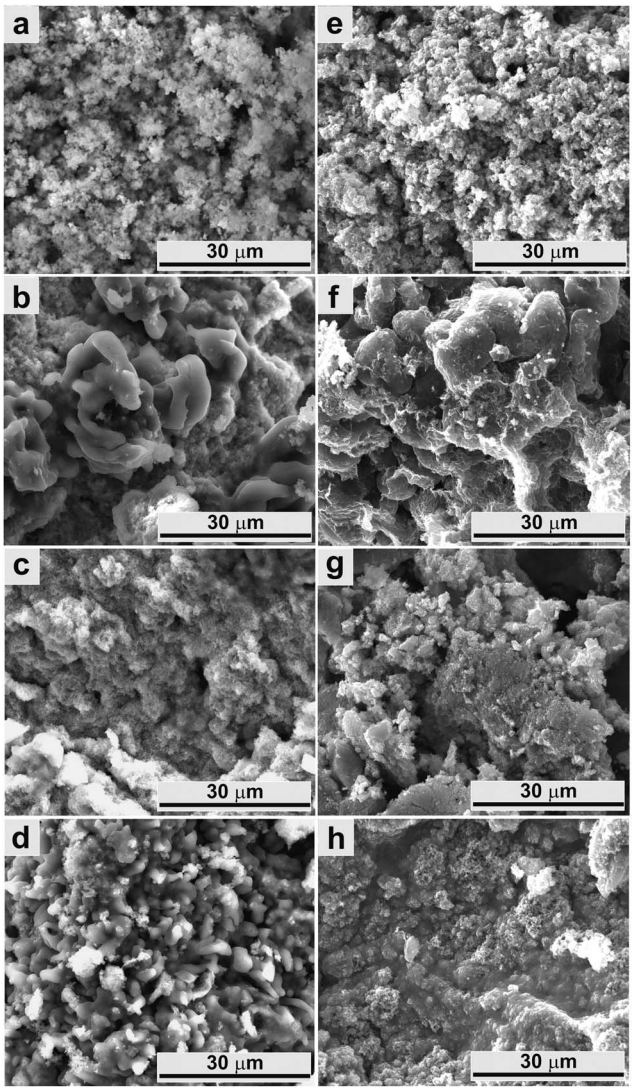

Fig. 1 SEM images of the Au foil covered with (a–d) $Ni(OH)_2$ and (e–h) NiO obtained (a and e) without modifier, in the presence of: (b and f) PVP, (c and g) 4-DMAP, and (d and h) PPST.

$$Ni^{2+} + 2OH^- \rightarrow Ni(OH)_2 \quad (3)$$

NiO was also obtained by annealing the as-prepared $Ni(OH)_2$ at 300 °C for 2 h, according to eqn (4):

$$Ni(OH)_2 \xrightarrow{\text{endothermic}} NiO + H_2O \quad (4)$$

Fig. 1 presents the SEM images of pure $Ni(OH)_2$ (Fig. 1a–d) and NiO (Fig. 1e–h) structures. The morphology of $Ni(OH)_2$ and NiO consists of particles of varied sizes and shapes, as a result of the addition of the modifiers to the solution during the synthesis. The most noticeable difference in morphology was observed for $Ni(OH)_2$ obtained in the presence of PVP. This material showed a non-uniform structure with a flower-like structure and grain particles. The nanostructures of the as-prepared $Ni(OH)_2$ were very similar to those of the NiO after calcinating at 300 °C, as shown in Fig. 1a and e. It seems that the annealing temperature was low enough to keep the nickel hydroxide nanostructures intact. $Ni(OH)_2$ prepared in the presence of polymers or 4-DMAP exhibited a different morphology than that of the products after the calcination process.

SEM studies showed different morphological characteristics and spectroscopic measurements (FT-IR and Raman) revealed that the nickel hydroxide (Fig. 2, panel 1a and 2a) and oxide materials (Fig. 2, panel 1b and 2b), exhibited the same structural characteristics. The FT-IR spectrum was used to determine the nature of the Ni samples before and after calcination. The FT-IR spectra of $Ni(OH)_2$ are presented in Fig. 2 (panel 1a) and collected in Table 1. The broad peak in the region between 3000 and 3800 cm^{-1} was ascribed to the stretch vibration of O–H groups in the nickel hydroxide and oxide lattices, indicating the presence of lattice water.[39] The band observed at 1617 cm^{-1} also indicated the presence of water. The NiO sample prepared at 300 °C showed some water in the lattice as well. It was already

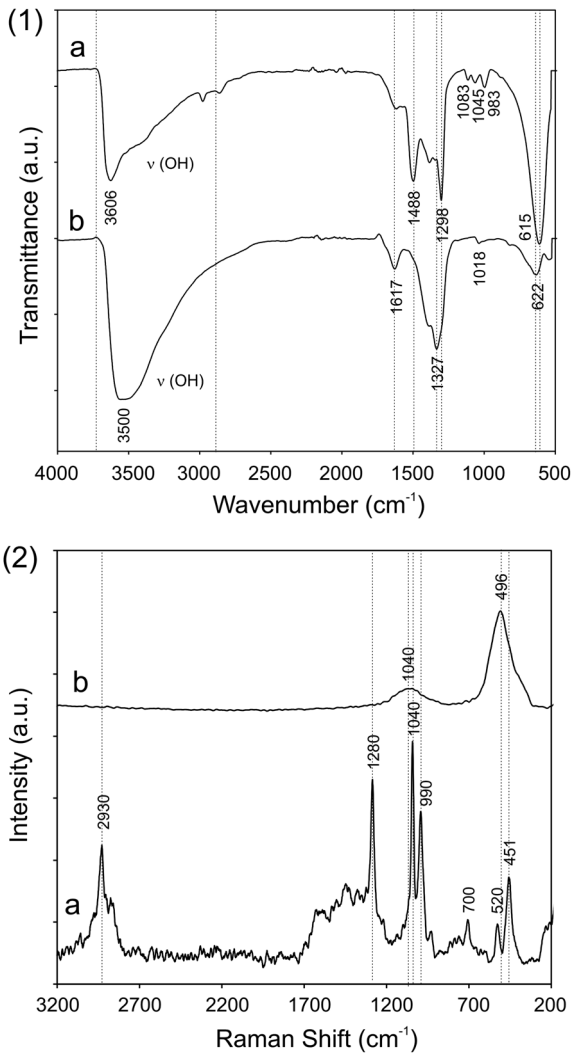

Fig. 2 Spectroscopic characteristics of (a) $Ni(OH)_2$ and (b) NiO obtained in the presence of 4-DMAP: (1) FTI-IR spectra in the range 4000–500 cm^{-1}. Spectra recorded at room temperature in a N_2 atmosphere. (2) Room temperature Raman spectra recorded for 514 nm excitation.

Table 1 Band frequencies and tentative assignment of the Raman and FTIR bands of $Ni(OH)_2$ and NiO[39–45]

FTIR (cm^{-1})		Raman (cm^{-1})		
$Ni(OH)_2$[a]	NiO[b]	$Ni(OH)_2$[a]	NiO[b]	Tentative assignment
3600				Vibrational stretching of hydroxyl group in the nickel hydroxide lattice
	3500			Hydroxyl group of the intercalated and adsorbed water
		2930		C–H stretching of aliphatic
1617	1617			Water angular deformation
1488				
1298	1327	1280		
1083				Nitrate anion
1045	1018	1040	1040	
983				
		900		Ni–O vibrational stretching
		700		Ni–O vibrational stretching
615	622			Ni–N vibrational stretching
		520		Ni–O vibrational stretching
		451	496	Ni–O vibrational stretching

[a] Prepared in the presence of 4-DMAP. [b] Annealed at 300 °C in an air atmosphere, 2 h.

reported that complete calcination occurs at 500 °C, and pure NiO is obtained.[40] Since Liu *et al.* reported that NiO calcinated at 300 °C has a higher specific capacitance than the one calcinated at 500 °C, we used 300 °C for our samples. Some of the bands assigned to the calcinated NiO are blue shifted compared to those of $Ni(OH)_2$ in bulk form due to a nanosize effect.[41] All of the Ni compounds have bands near the region of 1330–1300 and 1080–980 cm^{-1}, in which vibrations due to coordinated nitrate groups are known to occur.[42] On the basis of these observations, the band at about 620 cm^{-1} has been assigned to a Ni–N stretching vibration of the coordinated nitrate group.

The room temperature Raman spectrum of the mesoporous compounds showed bands at 520 and 451 cm^{-1}, which can be attributed to the stretching (Ni–OH) vibration (Fig. 2, panel 2a), and at 496 cm^{-1}, which is assigned to the stretch vibration of Ni–O (Fig. 2, panel 2b). The broad peak at 496 cm^{-1} is due to the Ni–O stretching mode (Fig. 2, panel 2b),[43] which can be identified as the $A_{2u}(T)$ lattice vibrations of nickel oxide.[44] Meanwhile, there are two other peaks (700 and 900 cm^{-1}) that arise from the mesoporous $Ni(OH)_2$ structures, which contain nanoparticles but not single crystalline material.[45]

The electrochemical applications of materials depend on the degree of particle agglomeration in the films, particle sizes, and other structural properties and defects on the surface of the nanostructures.[46] High surface areas are required for high performance supercapacitors. Since it was already observed that the crystal structure and morphology of $Ni(OH)_2$ or NiO nanoparticles has a significant influence on its electrochemical properties,[47] CV studies were performed for nickel oxides obtained in the presence of the different modifiers. The electrochemical characterizations in 1 M KOH electrolyte are shown in Fig. 3. The values of the capacitance for NiO varied between 58.9 and 105.6 F g^{-1} at 5 mV s^{-1}, depending on the modifier. The highest capacitance current was obtained for nickel oxides calcinated from $Ni(OH)_2$ prepared in the presence of 4-DMAP (Fig. 3). Thus this synthetic procedure was applied for the preparation of the CNO/4-DMAP/$Ni(OH)_2$ composite.

3.2. Preparation and characterization of the CNO/4-DMAP/$Ni(OH)_2$ and CNO/4-DMAP/NiO composites

The procedure for the modification of the CNOs surface with nickel hydroxide and oxide is presented in Scheme 1b. To introduce nickel particles on the CNO surfaces, (4-dimethylamino)pyridine (4-DMAP) was used as a modifier. 4-DMAP influenced the properties of the nickel hydroxide nanostructures and simultaneously led to a pronounced increase of the solubility of the carbon nanostructures in the protic solvents.

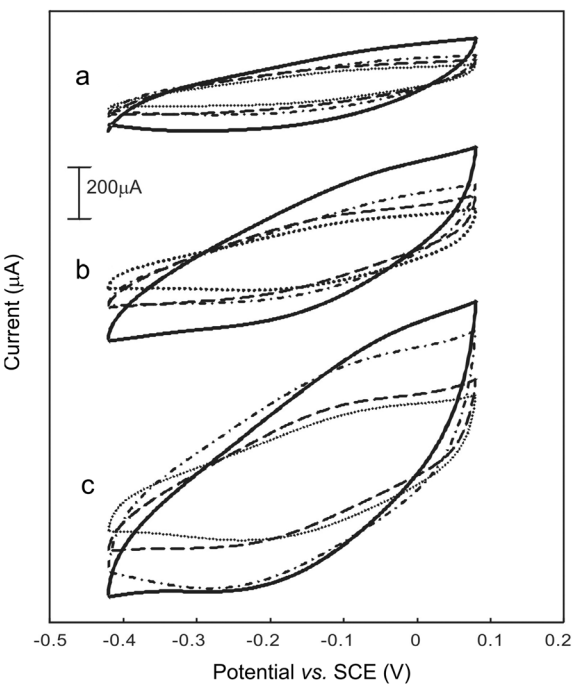

Fig. 3 Cyclic voltammograms of a GC electrode in 1 M KOH covered with NiO prepared without modifier (– – –), and in the presence of (– · –) PVP, (—) 4-DMAP or (····) PPST at (a) 5, (b) 20, and (c) 50 mV s^{-1} scan rates.

High-Resolution Transmission Electron Microscopy (HR-TEM) of the pure components of the composite: nickel hydroxide and oxide (Fig. 4a and b), was performed to determine the presence of inorganic structures in the composite. The HR-TEM images of $Ni(OH)_2$ clearly show (Fig. 4a) that the typical size of the particles is about 2–3 nm (structure 2, Fig. 4a). Fig. 4a showed also that $Ni(OH)_2$ reveals wrinkled surfaces (structure 1, Fig. 4a). $Ni(OH)_2$ exhibited similar flower shaped features with long needle-like type structures, which formed thin sheets. The unique sheet morphology with embedded mesoporous structures provides an ideal platform for fast ion transport, and has readily accessible surfaces for redox reactions.[15] The electron-diffraction pattern with a diffused halo ring indicates that these nanospheres (not shown) with irregular structures have amorphous structures. Recently it was reported that amorphous nickel hydroxide nanospheres exhibit high capacitance.[48] $Ni(OH)_2$ after calcination has more granular structures (structure 3, Fig. 4b). The HR-TEM observation of the CNO composites (Fig. 4c–e) showed both structures: inorganic and carbon-based in the composite matrix. As shown in Fig. 4c, the typical $Ni(OH)_2$ amorphous nanospheres (structure 1) and CNO particles (structure 4) are present in the composite. Both types of structures are also visible in the CNO/4-DMAP/NiO composite (structures 3 and 4, Fig. 4e).

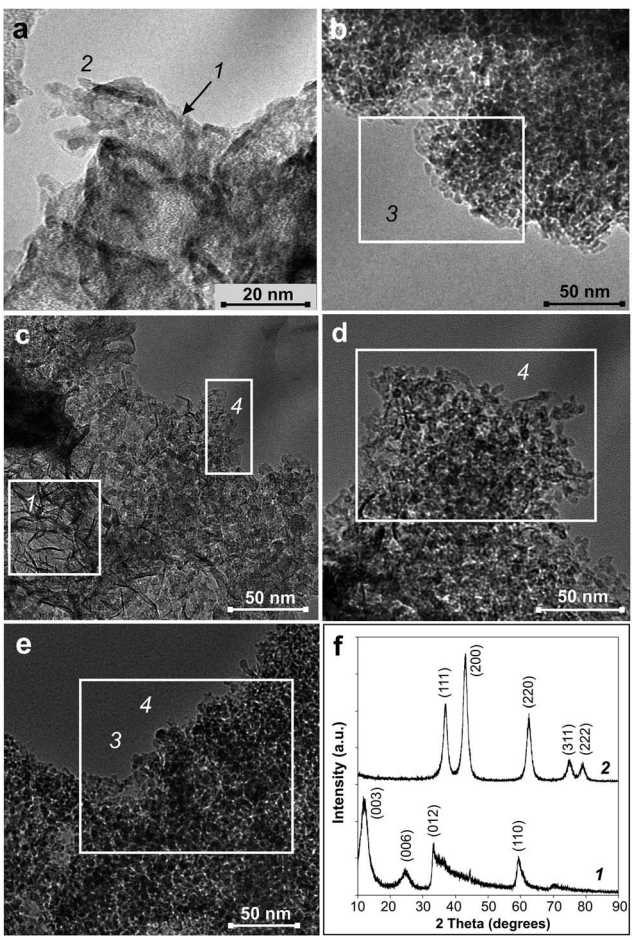

Fig. 4 HR-TEM images of (a) $Ni(OH)_2$, (b) NiO, (c and d) CNO/4-DMAP/$Ni(OH)_2$ and (e) CNO/4-DMAP/NiO. (f) XRD pattern of the (1) $Ni(OH)_2$ and (2) NiO products.

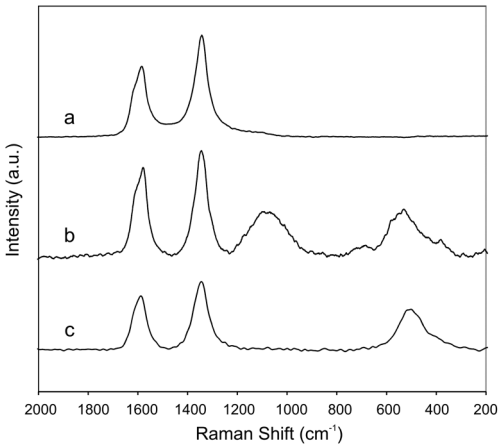

Fig. 5 Room temperature Raman spectra of (a) CNO and CNO composites obtained in the presence of 4-DMAP including (b) $Ni(OH)_2$ and (c) NiO, recorded for 514 nm excitation.

The XRD pattern of the $Ni(OH)_2$ and NiO products are presented in Fig. 4f. The large peak at 35.16° (003) reflected the typical turbostratic feature of α-$Ni(OH)_2$ (Fig. 4f, pattern 1).[49] All the diffraction peaks in Fig. 4f, pattern 1, are well indexed to the pure hexagonal α-$Ni(OH)_2$ phase (JCPDS card no. 03-0177): (003), (006), (012) and (110).[49] The typical wide-angle XRD pattern of the NiO sample obtained after calcination of α-$Ni(OH)_2$ is shown in Fig. 4e, pattern 2. Five well-defined peaks, corresponding to the (111), (200), (220), (311) and (222) reflections were observed. They can be indexed to the cubic NiO crystalline phase structure (JCPDS card no. 04-0835).[50]

Fig. 5 shows the Raman spectra of the CNO/4-DMAP/$Ni(OH)_2$ and CNO/4-DMAP/NiO composites and non-modified CNO for comparison. For all materials the strongest features are observed at about 1330 (D band) and 1580 cm^{-1} (G band). Moreover, in the spectral region from 300 cm^{-1} to 1200 cm^{-1} an additional two bands can also be observed, and according to the assignment by Dietz *et al.*, these correspond to one-phonon (1P) LO modes (at about 540 cm^{-1}) and two-phonon (2P) 2LO modes (1090 cm^{-1}) (Fig. 5b and c).[51] The phonon related part of the Raman spectra (1P and 2P bands) in the composite powders (Fig. 5b and c) is due to the presence of defects or surface effects.

Differential-thermogravimetric analyses (TGA-DTG-DTA) were performed to probe the thermal stability of pristine CNOs and their nickel composites in an air atmosphere. The temperature necessary for the removal of the porous carbon formed during the low-temperature annealing in an air atmosphere is lower than the decomposition temperature of the pristine carbon nanostructures. Fig. 6 shows the TGA-DTG-DTA scans under an air atmosphere at 10 °C min^{-1} for the CNO composites (Fig. 6, panels (1) i (2), curves d and e), and the reference materials: CNOs, $Ni(OH)_2$ and NiO (curves a–c, respectively). The onset oxidation and end temperatures are listed in Table 2, representing the initial weight loss, the maximum weight loss and the final weight in the TGA-DTG-DTA

graphs, respectively. The highest inflection temperature was observed for the pristine CNOs ($I_t = 610$ °C). There is no weight loss or very small loss at temperatures between 200 and 400 °C, showing the small content of amorphous carbon in the pristine CNO samples. Very sharp transitions are observed at 261 and 408 °C that correspond to the conversion of $Ni(OH)_2$ to NiO and H_2O (Fig. 6, panel 2, curve b).[52]

The same properties were also observed for the CNO/4-DMAP/$Ni(OH)_2$ composite (Fig. 6, panel 2, curve d). According to the TGA studies, we chose 300 °C as the annealing temperature for the production of NiO materials. The percentage of NiO and $Ni(OH)_2$ in the CNO composites can be estimated from the weight loss of the TGA curves. At temperatures of 260 and 400 °C, the weight percentages are 33 and 15%, which means the mass ratio of $Ni(OH)_2$ or NiO is about 4 : 1.

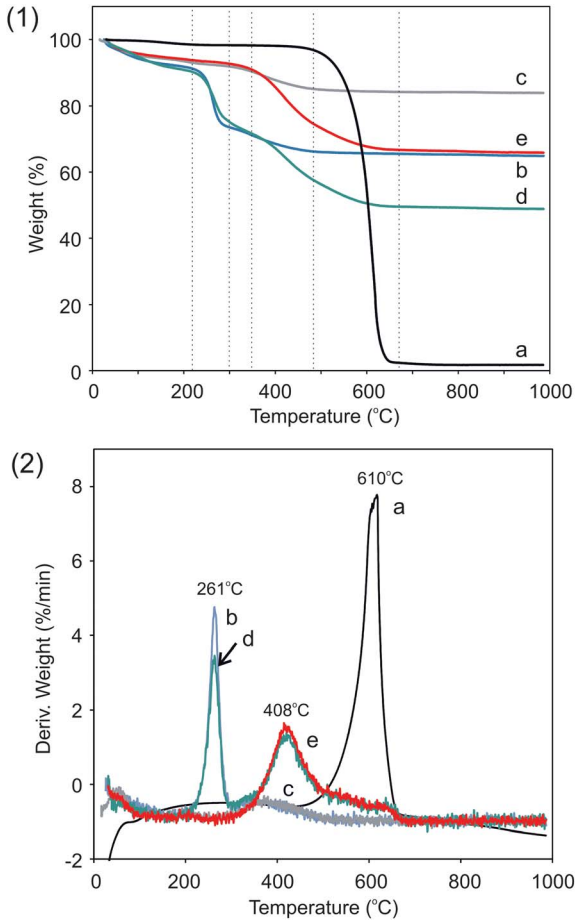

Fig. 6 (1) TGA and (2) DTG curves for (a) CNO (black line), (b) $Ni(OH)_2$ (blue line), (c) NiO (gray line), (d) CNO/4-DMAP/$Ni(OH)_2$ (green line), and (e) CNO/4-DMAP/NiO (red line) in an air atmosphere at 10 °C min^{-1}.

3.3. Morphology characterization and electrochemical studies

The capacitance values are strictly correlated with the nature and surface of the electrode–electrolyte interface. Generally, the larger the specific surface the higher the charge accumulation.[3,5] The CNO/4-DMAP/$Ni(OH)_2$ and CNO/4-DAMP/NiO composites were obtained *via* synthesis of the carbon nanostructures in the presence of 4-DMAP as modifier. The morphology and roughness of the synthesized CNO composite layers were studied by scanning electron microscopy. The results of the SEM studies are shown in Fig. 7. The morphology of the films formed by using modified CNO with Ni particles (Fig. 7d and e), does not differ significantly from that of films formed by non-functionalized nanostructures: $Ni(OH)_2$/NiO (Fig. 7b and c) or CNO (Fig. 7a).

Cyclic voltammetry was used to determine the electrochemical properties of NiO/$Ni(OH)_2$ and the CNO composites including such particles. As was previously observed, the capacitive performance of the carbon electrodes depends on their preparation protocol. Our previous preparation of solid films including CNO structures was based on the drop coating method using pure solvents. A drop of solution containing the dispersed carbon nanostructures were deposited on the electrode surface. After solvent evaporation, the electrode covered with the thin film was transferred to a solution containing the supporting electrolyte. These electrodes showed good mechanical and electrochemical stability, and some aggregation of the carbon-based materials was observed. The specific capacitance for the GC electrode covered with the pristine CNOs was equal to 7 F g^{-1}.[53] For the preparation of the films a conductive carbon paste was used to solubilize the non-modified and modified CNOs for further modification of the GC surface electrodes. The volume ratio of carbon paste to ethanol used was 1 : 6. A drop of 10 μL ethanol solution containing the dispersed CNOs was deposited on the electrode surface. After solvent evaporation, the electrode covered with the thin film was transferred to a solution with the supporting electrolyte. All voltammograms exhibit pseudorectangular profiles that are typical for double-layer capacitors (Fig. 8). These results

Table 2 The TGA-DTG-DTA results of CNOs and their $Ni(OH)_2$ and NiO composites

Sample	Onset temperature (°C)	Inflection temperature (°C)	End temperature (°C)	Total weight loss (%)
CNO	490	610	640	98
$Ni(OH)_2$[a]	261	200	490	33
NiO[a,b]	408	280	490	15
CNO/$Ni(OH)_2$[a]	261, 408	180	690	52
CNO/NiO[a,b]	408	240	680	34

[a] Prepared in the presence of 4-DMAP. [b] Annealed at 300 °C in an air atmosphere, 2 h.

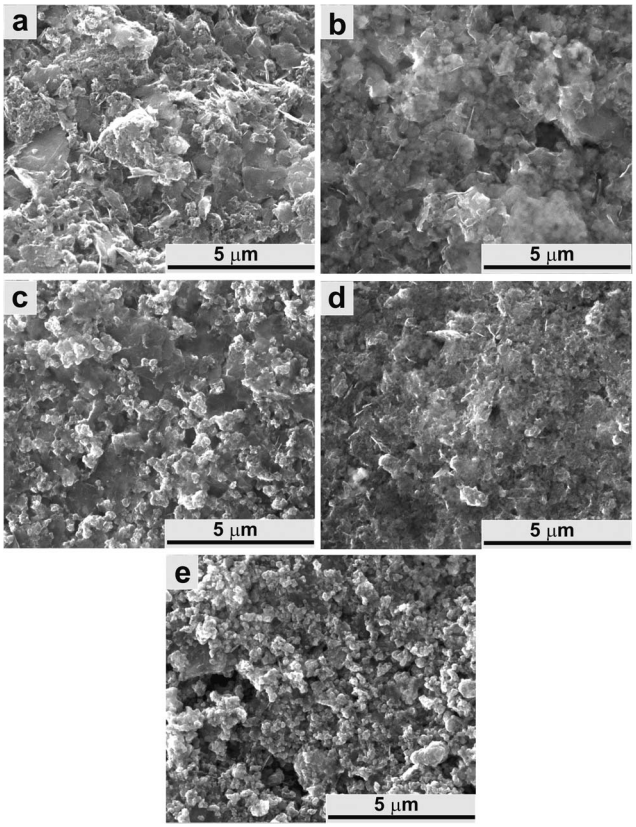

Fig. 7 SEM images of the Au foil covered with (a) CNOs, (b) $Ni(OH)_2$, (c) NiO, (d) CNO/4-DMAP/$Ni(OH)_2$, and (e) CNO/4-DMAP/NiO composites. The film was prepared as follows: 2 mg of active material (CNOs, $Ni(OH)_2$, NiO, CNO/4-DMAP/$Ni(OH)_2$ or CNO/4-DMAP/NiO) was dissolved in a solution containing conductive carbon paint and ethanol (volume ratio of 1 : 6).

indicate that the charge–discharge responses of the electric double layer are highly reversible and kinetically facile.[54] The capacitive current characteristics for pristine CNOs prepared in the presence of carbon paste was higher than those obtained by the drop coating method. Since the specific capacitance depends on the degree of particle agglomeration in the film, the conductive carbon paste allowed the preparation of good dispersions of CNOs in ethanol solution. The presence of conductive carbon paste is able to prevent the aggregation of

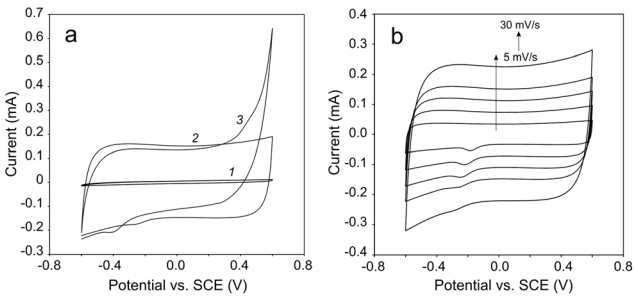

Fig. 8 (a) Cyclic voltammograms of a GC electrode covered with (1) carbon paste, (2 and 3) CNOs; CVs (1) and (2) in 0.1 M NaCl, and (3) in 1 M KOH; scan rates 5 mV s^{-1}; (b) cyclic voltammograms of a GC electrode covered with CNOs in 0.1 M NaCl with the different scan rates: 5, 10, 15, 20 and 30 mV s^{-1}.

Table 3 Specific capacitance of CNO-based materials obtained from the voltammetric studies[a]

	Specific capacitance (F g^{-1})[f] at different scan rates (mV s^{-1})				
Sample	5	10	15	20	30
CNO	30.6	37.9	38.5	39.1	39.1
	36.5[d]	43.3[d]	44.1[d]	44.7[d]	44.8[d]
$Ni(OH)_2$[b]	548.4	472.6	482.3	423.0	387.0
NiO[b,c]	83.6	82.3	72.4	78.2	77.2
CNO/$Ni(OH)_2$[b]	1225.2[e]	904.3[e]	871.3[e]	773.0[e]	727.4[e]
CNO/NiO[b,c]	290.6[e]	218.2[e]	222.5[e]	230.5[e]	272.5[e]

[a] Capacitance per gram of the composite. [b] Prepared in solution with 4-DMAP. [c] $Ni(OH)_2$ annealed at 300 °C in an air atmosphere, 2 h. [d] Capacitance in 0.1 M NaCl. [e] Capacitance per gram of CNOs into $Ni(OH)_2$ or NiO. [f] 1 M KOH.

CNOs caused by van der Waals interactions, consequently maintaining an electrochemically active surface area and a suitable porous structure. Adding conductive carbon paste for CNO film preparation was more effective than using pure solutions to enhance the performance of EDLC, with approximately 20 times larger specific capacitances, about 45 F g^{-1} (Table 3). The specific capacitance, C_s, was calculated based on the mass of the CNOs on the electrode surface, m, within the potential range, ΔE, (Fig. 8) according to the following equation:

$$C_s = \frac{\int i_c \, dt}{\Delta E \, m} \quad (5)$$

The CNO films show capacity ranges between 30 and 39 F g^{-1} in 1 M KOH (Fig. 8a (3)) and 36 and 45 in 0.1 M NaCl (Fig. 8b (2) and Table 3).

The CNO/4-DMAP/$Ni(OH)_2$ and CNO/4-DMAP/NiO composite films exhibited good mechanical and electrochemical stability under cyclic voltammetric conditions within the potential range from −0.60 to +0.60 V *versus* SCE. Fig. 9 shows the CV curves of the GC electrodes covered with inorganic/carbon-based film electrodes at different scan rates in 1 M KOH aqueous solution. A nickel oxide/hydroxide capacitor in alkaline solution relies on charge storage in the electric double layer at the electrode–electrolyte interface and charge storage in the host material through redox reactions on the surface and hydroxyl ion diffusion in the host material.[55] The redox peaks reveal the faradaic pseudocapacitive nature due to the Ni^{2+}/Ni^{3+} couple at the surface of $Ni(OH)_2$ (Fig. 9a) and NiO (Fig. 9b), according to the following equations:

$$Ni(OH)_2 + OH^- \leftrightarrow NiOOH + H_2O + e^- \quad (6)$$

$$NiO + OH^- \leftrightarrow NiOOH + e^- \quad (7)$$

The oxidation peak at 0.50 V (*vs.* SCE) is due to the conversion of NiO to NiOOH, whereas the reduction at 0.25 (*vs.* SCE) is due to the reverse reaction. A nickel hydroxide surface layer a few angstroms thick is formed.[56] The CNO/4-DMAP/$Ni(OH)_2$ composite shows similar electrochemical performance as

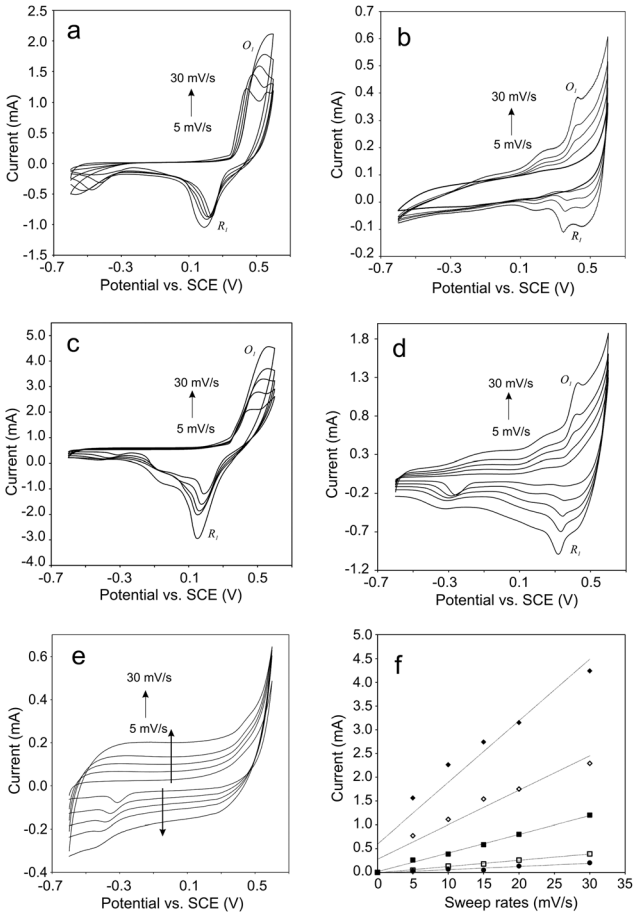

Fig. 9 Cyclic voltammograms of a GC electrode in 1 M KOH covered with: (a) $Ni(OH)_2$/4-DMAP, (b) NiO/4-DMAP, (c) CNOs/4-DMAP/$Ni(OH)_2$, (d) CNOs/4-DMAP/NiO and (e) CNOs with the different scan rates: 5, 10, 15, 20 and 30 mV s^{-1}; (f) dependence of the capacitive current with the sweep rate for: (●) CNOs, (□) NiO/4-DMAP, (■) CNOs/4-DMAP/NiO, (◇) $Ni(OH)_2$/4-DMAP and (◆) CNOs/4-DMAP/$Ni(OH)_2$ at +100 mV for CNOs and at O_1 peak.

$Ni(OH)_2$ (Fig. 9c), but the separation between oxidation and reduction peaks is decreased by 40 mV.

The capacitive current, i_c, is given by the following equation:

$$i_c = C_S v m \quad (8)$$

where C_s is the specific capacitance, m is the mass of the material deposited on the electrode surface, and v is the potential sweep rate. The values of the specific capacitances calculated from the dependence of the current with the scan rate for the different types of films (eqn (8)), are collected in Table 3. The values of the specific capacitances were calculated from the linear relationship of I–v plots (Fig. 9f).

The capacitive behavior of the CNOs/4-DMAP/$Ni(OH)_2$ and CNOs/4-DMAP/NiO composites are mainly attributed to the pseudocapacitive performance of nickel oxide or hydroxide, but the carbon nano-onions significantly increased the roughness and specific surface areas of the nanocomposite electrodes. The capacitances of CNO films are very low when compared to those of the composites. A specific capacitance between 30.6 and 39.1 F g^{-1} was obtained based on the CNOs mass. Much higher values of C_s for NiO or $Ni(OH)_2$ varied between 77.2 and 548.4 F g^{-1}. The role of the carbon nanostructures with high specific surface area is to supply more active sites for the redox reaction of $Ni(OH)_2$ or NiO.[57] A specific capacitance between 218.2 and 1225.2 F g^{-1} was obtained based on the composites mass, CNOs/4-DMAP/NiO or CNOs/4-DMAP/$Ni(OH)_2$, respectively. According to an earlier investigation,[58] the composite's structure is important for $Ni(OH)_2$/NiO to function as a fast charging and discharging supercapacitor and is responsible for the high pseudocapacitance value. Moreover, the presence of CNOs in the film results in an increase of the material's conductivity. The electrochemical performance of the CNO/4-DMAP/$Ni(OH)_2$ or CNO/4-DMAP/NiO composites is largely affected by the morphology and distribution of the $Ni(OH)_2$/NiO phase.[59]

In conclusion, CNOs improve the composite film properties, making them more active for faradaic reactions, thus conferring larger specific capacitances and better stabilities than for pristine $Ni(OH)_2$ or NiO.

4. Conclusion

We have shown that functionalization of carbon nano-onions with inorganic materials, such as $Ni(OH)_2$ or NiO, can be easily achieved. The structure and physico-chemical characterization of the composites was investigated by TEM, SEM, FT-IR, Raman and TGA-DTG-DTA. The CNO/4-DMAP/$Ni(OH)_2$ and CNO/4-DMAP/NiO films showed relatively porous structures on the electrode surface and exhibit typical pseudocapacitive behaviour, as well as good mechanical and electrochemical stability over a wide potential window, from +0.6 to −0.6 V (*vs.* SCE). The specific electrochemical capacitance of the CNO/4-DMAP/$Ni(OH)_2$ and CNO/4-DMAP/NiO composite films was significantly larger than for pure NiO or $Ni(OH)_2$. The highest specific capacitance of 1225.2 F g^{-1} was observed for the CNO/4-DMAP/$Ni(OH)_2$ composite films. The simple synthesis of these materials, their cation exchange properties, and their facile electrochemistry make them attractive for applications as electrodes for supercapacitors.

Acknowledgements

The authors thank A. Cyganiuk (Nicolaus Copernicus University, Torun, Poland) for XRD and TGA-DTG-DTA; J. Breczko (University of Bialystok) for FT-IR and Raman measurements. We gratefully acknowledge the financial support of the NCN, Poland, grant: #2011/01/B/ST5/06051 to M. E. P.-B. L. E. thanks the Robert A. Welch Foundation for an endowed chair, grant #AH-0033 and the US NSF, grants: CHE-1110967 and CHE-1124075. SEM and TEM, IR and Raman instruments were funded by the European Funds for Regional Development and the National Funds of Ministry of Science and Higher Education, as part of the Operational Programme Development of Eastern Poland 2007-2013, project: POPW.01.03.00-20-034/09-00.

Notes and references

1 R. Kötz and M. Carlen, *Electrochim. Acta*, 2000, **45**, 2483.

2 B. B. Owens and T. Osaka, *J. Power Sources*, 1997, **68**, 173; G. Wang, L. Zhang and J. Zhang, *Chem. Soc. Rev.*, 2012, **41**, 797; E. Frackowiak and F. Beguin, *Carbon*, 2001, **39**, 937; E. Frackowiak, *Phys. Chem. Chem. Phys.*, 2007, **9**, 1774.
3 S. Bose, T. Kuila, A. K. Mishra, R. Rajasekar, N. H. Kim and J. H. Lee, *J. Mater. Chem.*, 2012, **22**, 767.
4 J. Chmiola, G. Yushin, Y. Gogotsi, C. Portet, P. Simon and P. L. Taberna, *Science*, 2006, **313**, 1760; A. G. Pandolfo and A. F. Hollenkamp, *J. Power Sources*, 2006, **157**, 11; M. D. Levi, G. Salitra, N. Levy and D. Aurbach, *Nat. Mater.*, 2009, **8**, 872.
5 S. Park, H. Ch. Kim and T. D. Chung, *Analyst*, 2012, **137**, 3891.
6 F. Fusalba, H. A. Ho, L. Breau and D. Belanger, *Chem. Mater.*, 2000, **12**, 2581; K. K. Liu, Z. L. Hu, R. Xue, J. R. Zhang and J. J. Zhu, *J. Power Sources*, 2008, **179**, 858.
7 X. Dong, W. Shen, J. Gu, L. Xiong, Y. Zhu, H. Li and J. Shi, *J. Phys. Chem. B*, 2006, **110**, 6015; K. R. Prasad, K. Koga and N. Miura, *Chem. Mater.*, 2004, **16**, 1845; T. Y. Wie, C. H. Chen, H. C. Chien, S. Y. Lu and C. C. Hu, *Adv. Mater.*, 2010, **21**, 347.
8 M. Mastragostinoa, C. Arbizzani and F. Soavi, *Solid State Ionics*, 2002, **148**, 493.
9 J. Chang, J. Sun, C. Xu, H. Xu and L. Gao, *Nanoscale*, 2012, **4**, 6786.
10 Z. A. Hu, Y. L. Xie, Y. X. Wang, H. Y. Wu, Y. Y. Yang and Z. Y. Zhang, *Electrochim. Acta*, 2009, **54**, 2737.
11 M.-W. Xu, D.-D. Zhao, S.-J. Bao and H.-L. Li, *J. Solid State Electrochem.*, 2007, **11**, 1101; B. Wang, J. Park, C. Wang, H. Ahn and G. Wang, *Electrochim. Acta*, 2010, **55**, 6812.
12 J. Yan, T. Wei, W. Qiao, B. Shao, Q. Zhao, L. Zhang and Z. Fan, *Electrochim. Acta*, 2010, **55**, 6973.
13 M.-S. Wu, C.-Y. Huang and K.-H. Lin, *J. Power Sources*, 2009, **186**, 557.
14 Y. Wang and G. Z. Cao, *Key Eng. Mater.*, 2007, **336–338**, 2134.
15 X. Sun, G. Wang, J.-Y. Hwang and J. Lian, *J. Mater. Chem.*, 2011, **21**, 16581.
16 L. Dong, Y. Chu and W. Sun, *Chem.–Eur. J.*, 2008, **14**, 5064.
17 K. C. Liu and M. A. Anderson, *J. Electrochem. Soc.*, 1996, **143**, 124; K. W. Nam and K. B. Kim, *J. Electrochem. Soc.*, 2002, **149**, A346.
18 C. Z. Yuan, B. Gao and X. G. Zhang, *J. Power Sources*, 2007, **173**, 606; C. Z. Yuan, B. Gao, L. H. Su and X. G. Zhang, *Solid State Ionics*, 2008, **178**, 1859; F. Jiao, A. H. Hill, A. Harrison, A. Berko, A. V. Chadwick and P. G. Bruce, *J. Am. Chem. Soc.*, 2008, **130**, 5262.
19 H.-Y. Wu and H.-W. Wang, *Int. J. Electrochem. Sci.*, 2012, **7**, 4405.
20 M. S. Wu, M. J. Wang and J. J. Jow, *J. Power Sources*, 2010, **195**, 3950; V. Ganesh, S. Pitchumani and V. Lakshminarayanan, *J. Power Sources*, 2006, **158**, 1523; H. L. Wang, H. S. Casalongue, Y. Y. Liang and H. J. Dai, *J. Am. Chem. Soc.*, 2010, **132**, 7472; K. Liang, X. Tang and W. Hu, *J. Mater. Chem.*, 2012, **22**, 11062.
21 G.-W. Yang, C.-L. Xu and H.-L. Li, *Chem. Commun.*, 2008, 6537.
22 M. Salavati-Niasari, H. Seyghalkar, O. Amiri and F. Davar, *J. Cluster Sci.*, 2013, **24**, 365; L.-X. Yang, Y.-J. Zhu, H. Tong, Z.-H. Liang, L. Li and L. Zhang, *J. Solid State Chem.*, 2007, **180**, 2095; Y.-Z. Zheng, H.-Y. Ding and M.-L. Zhang, *Mater. Res. Bull.*, 2009, **44**, 403.
23 A. M. Soleimanpour and A. H. Jayatissa, *Mater. Sci. Eng. C*, 2012, **32**, 2230.
24 M.-S. Wu, Y.-A. Huang, C.-H. Yang and J.-J. Jow, *Int. J. Hydrogen Energy*, 2007, **32**, 4153.
25 J. D. Desai, S.-K. Min, K.-D. Jung and O.-S. Joo, *Appl. Surf. Sci.*, 2006, **253**, 1781.
26 C. C. Hu, W. C. Chen and K. H. Chang, *J. Electrochem. Soc.*, 2004, **151**, A281; H. Kuan-Xin, W. Quan-Fu, Z. Xiao-Gang and W. Xin-Lei, *J. Electrochem. Soc.*, 2006, **153**, A1568–A1574.
27 X. Huang, X. Qi, F. Boey and H. Zhang, *Chem. Soc. Rev.*, 2012, **41**, 666; Ch.-W. Huang, Ch.-T. Hsieh, P.-L. Kuo and H. Teng, *J. Mater. Chem.*, 2012, **22**, 7314; M. Wu, G. A. Snook, V. Gupta, M. Shaffer, D. J. Fray and G. Z. Chen, *J. Mater. Chem.*, 2005, **15**, 2297; R. B. Moghaddam and P. G. Pickup, *Phys. Chem. Chem. Phys.*, 2010, **12**, 4733; N. A. Kumar, H. J. Choi, A. Bund, J.-B. Baek and Y. T. Jeong, *J. Mater. Chem.*, 2012, **22**, 12268; J. H. Park, O. O. Park, K. H. Shin, Ch. S. Jin and J. H. Kim, *Electrochem. Solid-State Lett.*, 2002, **5**, H7; S. Arai, M. Endo, T. Sato and A. Koide, *Electrochem. Solid-State Lett.*, 2006, **9**, C131; S. Arai, T. Saito and M. Endo, *J. Electrochem. Soc.*, 2007, **154**, D530; T. Okumura, T. Sugiyo, T. Inoue, M. Ikegami and T. Miyasaka, *J. Electrochem. Soc.*, 2013, **160**, H155; Z. Tai, J. Lang, X. Yan and Q. Xue, *J. Electrochem. Soc.*, 2012, **159**, A485.
28 R. P. Deo, N. S. Lewrence and J. Wang, *Analyst*, 2004, **129**, 1076; C.-T. Hsieh, Y.-W. Chou, W.-Y. Chen and J.-Y. Lin, *Int. J. Hydrogen Energy*, 2007, **32**, 3457; A. S. Adekunle and K. I. Ozoemena, *Electrochim. Acta*, 2008, **53**, 5774; A. Czerwinski, M. Dmochowska, M. Grden, M. Kopczyk, G. Wojcik, G. Mlynarek, J. Kolata and J. M. Skowronski, *J. Power Sources*, 1999, **77**, 28; K. T. Roro, N. Tile and A. Forbes, *Appl. Surf. Sci.*, 2012, **258**, 7174; Ch. Xu, J. Sun and L. Gao, *J. Power Sources*, 2011, **196**, 5138; G.-H. Yuan, Z.-H. Jiang, A. Aramata and Z. Gao, *Carbon*, 2005, **43**, 2913.
29 V. L. Kuznetsov, A. L. Chuvilin, Y. V. Butenko, I. Y. Malkov and V. M. Titov, *Chem. Phys. Lett.*, 1994, **222**, 343; J. Qian, C. Pantea, J. Huang, T. W. Zerda and Y. Zhao, *Carbon*, 2004, **42**, 2691; Q. Zou, Y. G. Li, B. Lv, M. Z. Wang, L. H. Zou and Y. C. Zhao, *Inorg. Chem.*, 2010, **46**, 127; A. Palkar, F. Melin, C. M. Cardona, B. Elliott, A. K. Naskar, D. D. Edie, A. Kumbhar and L. Echegoyen, *Chem.–Asian J.*, 2007, **2**, 625.
30 S. Sek, J. Breczko, M. E. Plonska-Brzezinska, A. Z. Wilczewska and L. Echegoyen, *ChemPhysChem*, 2013, **14**, 96.
31 M.-S. Wang, D. Goldberg and Y. Bondo, *ACS Nano*, 2010, **4**, 4396.
32 S. Tomita, M. Fujii and S. Hayashi, *Phys. Rev. B: Condens. Matter Mater. Phys.*, 2002, **66**, 245424; V. L. Kuznetzov, S. I. Moseenkov, K. V. Elumeeva, T. V. Larina, V. F. Anufrienko, A. I. Romanenko, O. B. Anikeeva and E. N. Tkachev, *Phys. Status Solidi B*, 2011, **248**, 2572; T. Cabioc'h, S. Camelio, L. Henrard and Ph. Lambin, *Eur. Phys. J. B*, 2000, **18**, 535.
33 M. E. Plonska-Brzezinska, D. M. Brus, J. Breczko and L. Echegoyen, *Chem.–Eur. J.*, 2013, **19**, 5019; J. Breczko,

M. E. Plonska-Brzezinska and L. Echegoyen, *Electrochim. Acta*, 2012, **72**, 61; J. Luszczyn, M. E. Plonska-Brzezinska, A. Palkar, A. T. Dubis, A. Simionescu, D. T. Simionescu, B. Kalska-Szostko, K. Winkler and L. Echegoyen, *Chem.–Eur. J.*, 2010, **16**, 4870.

34 Y. Liu, R. L. Vander Wal and V. N. Khabashesku, *Chem. Mater.*, 2007, **19**, 778.

35 J. K. McDonough, A. I. Frolov, V. Presser, J. Niu, Ch. H. Miller, T. Ubieto, M. V. Federov and Y. Gogotsi, *Carbon*, 2012, **50**, 3298; C. Portret, G. Yushin and Y. Gogotsi, *Carbon*, 2007, **45**, 2511; G. Salitra, A. Soffer, L. Eliad, Y. Cohen and D. Aurback, *J. Electrochem. Soc.*, 2000, **147**, 2486; C. Vix-Guterl, E. Frackowiak, K. Jurewicz, M. Friebe, J. Parmantier and F. Beguin, *Carbon*, 2005, **43**, 1293; L. Eliad, G. Salitra, A. Soffer and D. Aurbach, *Langmuir*, 2005, **21**, 3198; R. Lin, P. Huang, J. Segalini, C. Largeot, P. L. Taberna, J. Chmiola, Y. Gogotsi and P. Simon, *Electrochim. Acta*, 2009, **54**, 7025; E. Raymundo-Pinero, K. Kierczek, J. Machnikowski and F. Begiun, *Carbon*, 2006, **44**, 2498; J. Chmiola, C. Largeot, P.-L. Taberna, P. Simon and Y. Gogotsi, *Angew. Chem., Int. Ed.*, 2008, **47**, 3392; M. E. Plonska-Brzezinska, A. Palkar, K. Winkler and L. Echegoyen, *Electrochem. Solid-State Lett.*, 2010, **13**, K35; M. E. Plonska-Brzezinska, J. Mazurczyk, J. Breczko, B. Palys, A. Lapinski and L. Echegoyen, *Chem.–Eur. J.*, 2012, **18**, 2600; E. Gradzka, K. Winkler, M. Borowska, M. E. Plonska-Brzezinska and L. Echegoyen, *Electrochim. Acta*, 2013, **96**, 274; J. Breczko, K. Winkler, M. E. Plonska-Brzezinska, A. Villalta-Cerdas and L. Echegoyen, *J. Mater. Chem.*, 2010, **20**, 7761.

36 Y.-G. Wang, L. Yu and Y.-Y. Xia, *J. Electrochem. Soc.*, 2006, **153**, A743.

37 X. Liu, S. W. Or, Ch. J., Y. Lv, Ch. Feng and Y. Sun, *Carbon*, 2013, **60**, 215.

38 R. L. Penn and J. F. Banfield, *Science*, 1998, **281**, 969; B. Liu, S. H. Yu, L. J. Li, F. Zhang, Q. Zhang, M. Yoshimura and P. K. Shen, *J. Phys. Chem. B*, 2004, **108**, 2788; B. J. Xi, S. L. Xiong, D. C. Xu, J. F. Li, H. Y. Zhou, J. J. Y. Pan and Y. T. Qian, *Chem.–Eur. J.*, 2008, **14**, 9786; Ch. Yuan, X. Zhang, L. Su, B. Gao and L. Shen, *J. Mater. Chem.*, 2009, **19**, 5772.

39 M. B. J. G. Freitas, *J. Power Sources*, 2001, **93**, 163; M. B. J. G. Freitas, R. K. Silva Silva, D. M. A. Rozario and P. G. Manoel, *J. Power Sources*, 2007, **165**, 916.

40 X.-M. Liu, X.-G. Zhang and S.-Y. Fu, *Mater. Res. Bull.*, 2006, **41**, 620.

41 A. J. Hunt, T. R. Steyer and D. R. Huffman, *Surf. Sci.*, 1973, **36**, 454.

42 C. W. Fraxk and L. B. Rogers, *Inorg. Chem.*, 1966, **5**, 622.

43 S. I. Cordoba-Torresi, A. Hugot-Le Goff and S. Joiret, *J. Electrochem. Soc.*, 1991, **138**, 1554.

44 J. Yan, W. Sun, T. Wei, Q. Zhang, Z. Fan and F. Wei, *J. Mater. Chem.*, 2012, **22**, 11494.

45 B. Li, M. Ai and Z. Xu, *Chem. Commun.*, 2010, **46**, 6267.

46 P. Simon and Y. Gogotsi, *Philos. Trans. R. Soc., A*, 2010, **368**, 3457.

47 M. C. Bernard, R. Cortes, M. Keddam, H. Takenouti, P. Bernard and S. Senyarich, *J. Power Sources*, 1996, **63**, 247; K. Watanabe and T. Kikuoka, *J. Appl. Electrochem.*, 1995, **25**, 219; D. E. Reisner, A. J. Salkind, P. R. Strutt and T. D. Xiao, *J. Power Sources*, 1997, **65**, 231.

48 H. B. Li, M. H. Yu, F. X. Wang, P. Liu, Y. Liang, J. Xiao, C. X. Wang, Y. X. Tong and G. W. Yang, *Nat. Commun.*, 2013, **4**, 1894.

49 B. C. Cornilsen, P. J. Karjala and P. L. Loyselle, *J. Power Sources*, 1988, **22**, 351; H. B. Liu, L. Xiang and Y. Jin, *Cryst. Growth Des.*, 2006, **6**, 283; M. Salavati-Niasari, H. Seyghalkar, O. Amiri and F. Davar, *J. Cluster Sci.*, 2013, **24**, 365.

50 Y.-z. Zheng, H.-y. Ding and M.-l. Zhang, *Mater. Res. Bull.*, 2009, **44**, 403; X.-M. Liu, X.-G. Zhang and S.-Y. Fu, *Mater. Res. Bull.*, 2006, **41**, 620; Ch. Yuan, J. Li, L. Hou, L. Yang, L. Shen and X. Zhang, *Electrochim. Acta*, 2012, **78**, 532.

51 R. E. Dietz, W. F. Brinkman, A. E. Meixner and H. J. Guggenheim, *Phys. Rev. Lett.*, 1971, **27**, 81.

52 W. Xing, F. Li, Z. F. Yan and G. Q. Lu, *J. Power Sources*, 2004, **134**, 324.

53 M. E. Plonska-Brzezinska, M. Lewandowski, M. Błaszyk, A. Molina-Ontoria, T. Luciński and L. Echegoyen, *ChemPhysChem*, 2012, **13**, 4134.

54 S. R. S. Prabaharan, R. Vimala and Z. Zainal, *J. Power Sources*, 2006, **161**, 730.

55 R. Bernard, C. F. Randell and F. L. Tye, *J. Appl. Electrochem.*, 1980, **10**, 109.

56 P. A. Nelson and J. R. Owen, *J. Electrochem. Soc.*, 2003, **150**, A1313; K. W. Nam, E. S. Lee, J. H. Kim, Y. H. Lee and K. B. Kim, *J. Electrochem. Soc.*, 2005, **152**, A2123; I. Bouessay, A. Rougier and M. Tarascon, *J. Electrochem. Soc.*, 2004, **151**, H145; K. W. Nam, K. H. Kim, E. S. Lee, W. S. Yoon, X. Q. Yang and K. B. Kim, *J. Power Sources*, 2008, **182**, 642.

57 Y.-z. Zheng and M.-l. Zhang, *ECS Trans.*, 2007, **2**(8), 51.

58 C. Yuan, X. Zhang, L. Su, B. Gao and L. Shen, *J. Mater. Chem.*, 2009, **19**, 5772.

59 P. Lin, Q. She, B. Hong, X. Liu, Y. Shi, Z. Shi, M. Zheng and Q. Dong, *J. Electrochem. Soc.*, 2010, **157**, A818.